Tellus (1991), *43B*, 420–433

Reflectivities of uniform and broken layered clouds

By JAMES A. COAKLEY, JR., *Department of Atmospheric Sciences, Oregon State University, Corvallis, OR 97331-2209, USA*

(Manuscript received 15 June 1990; in final form 8 February 1991)

ABSTRACT

1 km AVHRR imagery data from the NOAA satellites, collected during the FIRE Marine Stratocumulus Intensive Field Observations, were used to determine differences between the reflectivities of uniform, layered clouds and those of broken clouds taken from the same layers. Observations for the 0.63 μm channel indicated that regardless of the viewing geometry obtained with the polar orbiters, the average reflectivities of broken clouds were approximately 80–85% of the reflectivities of the same clouds when they formed uniform layers. Furthermore, the anisotropy of radiation reflected by uniform clouds appeared to be no different than that reflected by the broken clouds. Consequently, if the uniform, layered clouds observed in this study reflect according to plane-parallel theory, then the reflectivities of broken clouds could be approximated by simply reducing the values obtained with plane-parallel theory. For observations in the 3.7 μm channel, the average reflectivities of the broken clouds were generally larger than the reflectivities of the uniform, layered clouds. Furthermore, the anisotropy of radiation reflected by broken clouds differed from that of the radiation reflected by uniform clouds. The reduced reflectivity at visible wavelengths for broken clouds may explain the 10% discrepancy between pre-satellite era estimates of the earth's albedo and satellite estimates. Furthermore, while the differences in reflectivities between uniform and broken clouds are qualitatively consistent with Monte Carlo simulations of finite cloud effects, they are also consistent with plane-parallel radiative transfer models in which the central portions of clouds contain relatively large concentrations of liquid water distributed among relatively large droplets, while the edges of clouds contain relatively low concentrations of liquid water distributed among relatively small droplets.

1. Introduction

Clouds reflect the major portion of incident sunlight that is reflected by the earth-atmosphere system. Through this reflected radiation, clouds gain a formidable hold on the earth's radiation budget and climate. In calculations of the reflected radiation clouds are often treated as being spatially homogeneous, isotropic, semi-infinite and plane-parallel. For over a decade, however, Monte Carlo simulations of scattering within clouds (Mckee and Cox, 1974; Aida, 1977) as well as analytic studies (Davies, 1978) have shown that the reflectivities of clouds that have sides differ substantially from those predicted by plane-parallel radiative transfer theory. Nevertheless, owing to the complexity of three-dimensional radiative transfer, the lack of realistic models for the spatial distribution of clouds or for the distribution of scatterers within clouds, treatments of finite cloud effects have been restricted to simple, idealistic cloud geometries such as cubes, cylinders, domes, etc. While the treatments for such idealized clouds have led to reports of the differences which might be expected between plane-parallel radiative transfer calculations and those for more realistic geometries, they have not attempted to estimate what differences might be expected between the reflectivities of real clouds and those predicted by plane-parallel theory. Here satellite observations, which were collected as part of the First International Satellite Cloud Climatology Project Regional Experiment (FIRE) Intensive Field Observations (IFO) for marine stratocumulus, are used to determine the effects of brokenness on cloud reflectivities.

Reflected radiation observed with satellite radiometers has been used by others to report on finite cloud effects. Reynolds et al. (1978) found, in

a case study of cumulus clouds over Colorado, that the reflectivities of larger clouds were higher than those of smaller clouds. The higher reflectivities for the larger clouds was qualitatively consistent with the results of Monte Carlo simulations which showed that leakage of photons through the sides of clouds and subsequent absorption by the surface caused the reflectivities of finite clouds to be smaller than those predicted for equivalent plane-parallel clouds. Minnis (1989) found higher apparent cloud fractions at larger view angles as well as higher cloud reflectivities at larger view angles when individual scenes were viewed simultaneously by more than one satellite. Coakley and Davies (1986) showed that while the reflectivities of broken clouds seemed to be smaller than those for uniform extensive clouds at visible wavelengths, for which hydrometeors are nonabsorbing, the reflectivities of broken clouds were higher than those of uniform clouds at 3.7 μm, where the hydrometeors absorb radiation. These differences could be qualitatively explained through Monte Carlo simulations. It was noted, however, that the differences might also be explained on the basis of plane-parallel radiative transfer theory if the column concentrations and sizes of cloud droplets increased systematically from the edges of clouds to the centers.

In this study, the spatial coherence method (Coakley and Bretherton, 1982; Coakley and Baldwin, 1984) is used to isolate single-layered systems of marine stratocumulus that span several hundred kilometers, and then to separate the clouds in these systems into those which are evidently unbroken for several kilometers from those that are broken on scales of one kilometer or less. The extensive, uniform, layered clouds are taken to be planar and their reflectivities are taken to represent those of plane-parallel clouds. These reflectivities are compared with those of nearby broken clouds which are part of the same cloud system. As in the previous study, the reflectivities are compared at 0.63 μm, where cloud droplets are nonabsorbing, and at 3.7 μm, where the droplets absorb and the single-scattering albedo is $\sim$0.9.

2. Data analysis

The Fire Marine Stratocumulus Intensive Field Observations (IFO) took place off the coast of southern California between 29 June and 18 July, 1987. During this period, 1 km data from the AVHRRs on the NOAA-9 and NOAA-10 satellites were collected. NOAA-9 had overpass times of approximately 1430 and 0230 LT, and NOAA-10

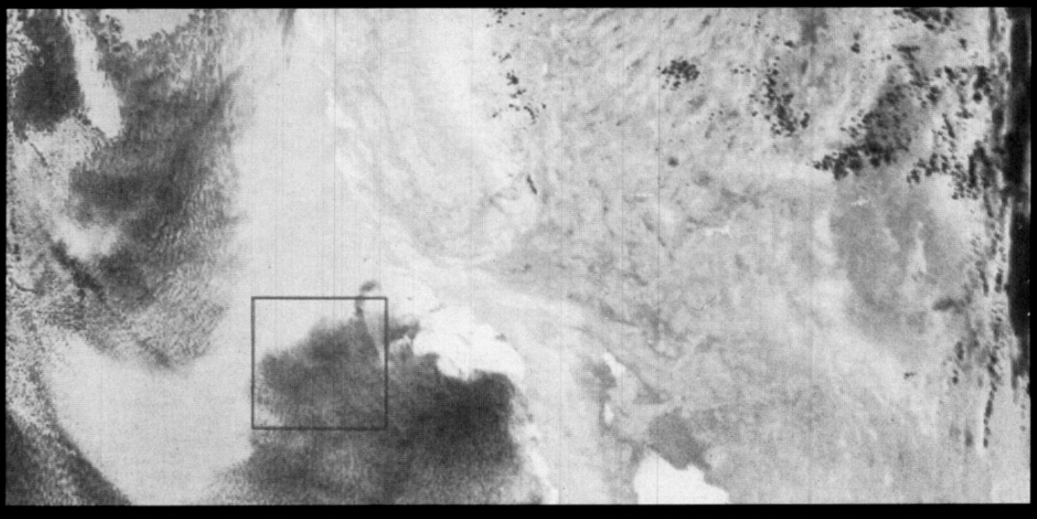

Fig. 1. Image constructed from 0.63 μm reflectivities obtained from NOAA-9 AVHRR on 7 July 1987 at 2242 GMT. The image shows the data collection typical of a polar orbiter overpass during the FIRE Marine Stratocumulus IFO. The square region in the figure indicates the portion of the region for which analyzed results are presented in Fig. 3.

had overpass times of approximately 0730 and 1930 LT. The observations were analyzed using the spatial coherence method.

Fig. 1 shows an image constructed from 0.63 μm reflectivities obtained with the NOAA-9 overpass at 2242 GMT on July 7 during the FIRE IFO. Fig. 2 shows the geographic location of the image and the division of the region into the 64×64 scan line $\times$ scan spot squares which are termed "$(60\ \text{km})^2$ subframes" because of their approximate 60 km scale at nadir. Within each subframe reflectivities for uniform layered clouds and differences in reflectivities between uniform and broken clouds are obtained. Only data over oceans was included in the analysis of cloud reflectivities. Fig. 3 shows an example of spatial coherence analysis for a 256×256 scan line $\times$ scan spot scene which is termed a "$(250\ \text{km})^2$ frame." The scene is outlined by the box in the image shown in Fig. 1. Each point in the figure represents 16 of the 1 km AVHRR fields of view taken from 4×4 scan line $\times$ scan spot arrays. Fig. 3a shows an arch which is typical of such diagrams. The single arch indicates that the observations are for a single-layered cloud system. Where the local standard deviations are small, as in the feet of the arch, the fields of view are either overcast (the foot exhibiting the lower emission at 11 μm), or cloud-free (the foot exhibiting the higher emission). Points in the body of the arch indicate radiances associated with broken clouds. In the case shown, a sizeable fraction of the $(4\ \text{km})^2$ pixel arrays within the $(250\ \text{km})^2$ region contain clouds that are broken at least at the 1 km scale corresponding to the spatial resolution of the instrument.

The spatial coherence analysis was performed in order to determine which fields of view were cloud-free, which were overcast and which contained broken clouds. Once the fields of view had been separated into these three categories, the mean reflectivities at 0.63 μm and radiances at 3.7 μm and 11 μm for cloud-free and overcast fields of view as well as the means for all fields of view within $(60\ \text{km})^2$ subframes that constituted each $(250\ \text{km})^2$ frame were preserved. Within each subframe, the radiance for overcast fields of view were

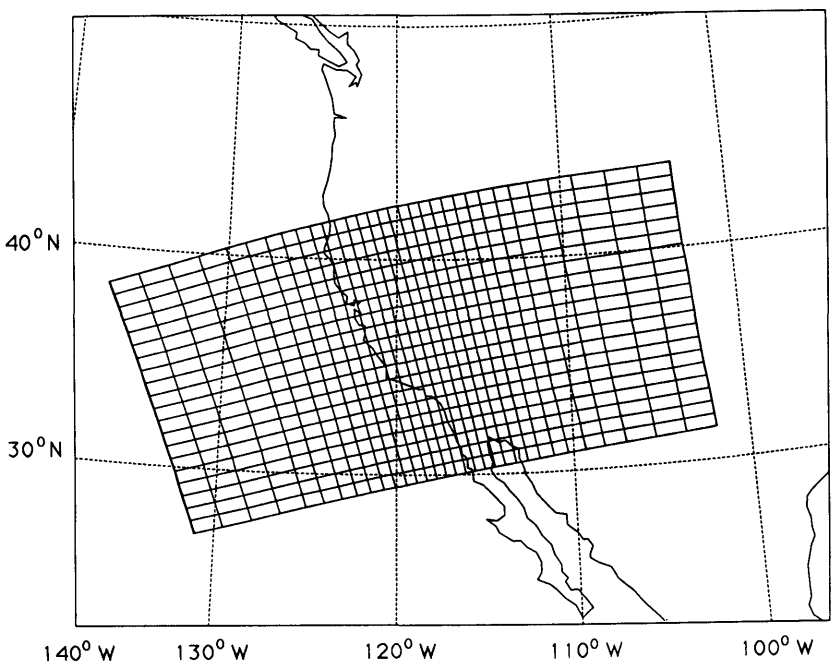

Fig. 2. Geographic location of image shown in Fig. 1. The boxes represent the "$(60\ \text{km})^2$ subframes" within which reflectivities for uniform, layered clouds and differences in reflectivities between uniform and broken clouds are obtained.

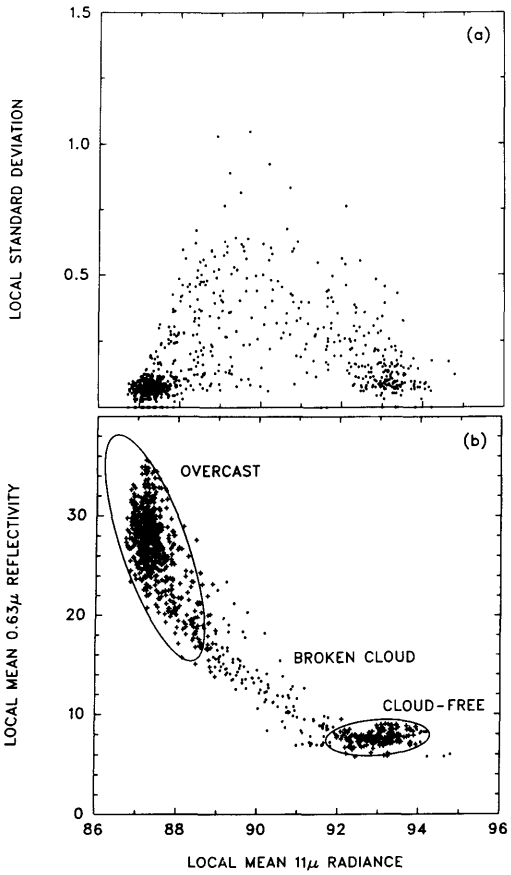

Fig. 3. Spatial coherence analysis of 11 μm radiances (mW m^{-2} sr^{-1} cm) (a) and 0.63 μm reflectivities (%) and 11 μm radiances (b) for the (250 km)^2 region within the square shown in Fig. 1. Each point in the figure gives values calculated for a 4×4 array of (1 km)^2 AVHRR pixels. The arch in (a) indicates that the clouds form a single-layered system of marine stratocumulus. The crosses in (b) are associated with (4 km)^2 arrays that are overcast or cloud-free; the dots are associated with arrays which contain clouds that are broken on scales smaller than the 1 km resolution of the AVHRR.

taken to represent those of a uniform cloud layer. To obtain the reflectivity of the broken clouds, r'_c, the mean reflectivity for the fields of view containing broken clouds was assumed to be given by

$$r' = (1 - A'_c)\, r_s + A'_c r'_c, \tag{1}$$

where A'_c is the fractional cloud cover for the fields of view containing broken clouds and r_s is the reflectivity of the cloud-free background. The fractional cloud cover is given in terms of the 11 μm radiances by

$$A'_c = \frac{I' - I_s}{I_c - I_s}\ , \tag{2}$$

where I' is the mean radiance for the fields of view containing broken clouds; I_c is the emission for overcast fields of view and I_s is the emission for cloud-free fields of view. The fractional cloud cover obtained through (2) is reasonably accurate provided that the clouds are opaque at 11 μm and that the clouds form a single layer with a definite cloud-top altitude as opposed to a system with a distribution of cloud top altitudes. For marine stratocumulus, these conditions are usually met (Coakley and Davies, 1986).

The linear relationship between reflectivity and cloud cover in (1) is justified by the observations shown in Fig. 3b. The figure shows the relationship between 0.63 μm reflectivities and 11 μm radiances for the data presented in Fig. 3a. Ellipses have been drawn around points which have been identified as cloud-free and overcast. The remaining observations are due to broken clouds. For the cloud-free foot the 0.63 μm reflectivity is relatively constant, as is often the case for cloud-free ocean scenes localized within a (250 km)^2 region and away from specular reflection in the area of sunglint. The width of the cloud-free foot at 11 μm suggests that the portion of the (250 km)^2 region that is cloud-free, evidently the northwest quadrant as shown in Fig. 1, is subject to either surface temperature gradients or gradients in atmospheric water vapor, or both. For broken cloud fields the figure shows that the local mean reflectivity appears to be a linear function of the 11 μm radiance for small to moderate departures from the values associated with the cloud-free fields of view. As the radiances approach those of overcast fields of view, departures from a linear relationship become noticeable. Presumably, the growth of a nonlinear contribution is the result of cloud-to-cloud reflection at visible wavelength as gaps between the clouds disappear. Monte Carlo simulations of the radiative processes in arrays of finite clouds indicate that the nonlinear contribution becomes noticeable for cloud cover fractions greater than about 0.6 for overhead sun (Welch and Wielicki, 1986). The linear relationship for small cloud cover and

nonlinear relationship for large cloud cover was noted in earlier studies (Coakley and Davies, 1986).

Thus, for each $(60\ \text{km})^2$ subframe (1) is inverted to obtain r_c', the reflectivity associated with broken clouds. These reflectivities are then compared with those of overcast fields of view within the same $(60\ \text{km})^2$ subframe so that the uniform and broken clouds are as identical as possible. Differences in reflectivities are then taken to represent the effects of brokenness on the reflected sunlight. The effects include those of the sides on radiative transfer as well as those like a reduction in cloud liquid water amount for broken clouds which may be partly responsible for the destruction of the layer in the first place.

Similar reflectivities are obtained for radiation reflected at 3.7 μm. To obtain the reflected radiation, the contribution to the observed radiance due to thermal emission is removed on the basis of the emission observed at 11 μm. The relationship between 3.7 and 11 μm emission is derived from nighttime observations for cloud-free and overcast fields of view obtained with the NOAA-9 AVHRR. The observations are shown in Fig. 4 as a function of satellite view angle. Based on the nighttime observations, the emission temperature at 3.7 μm is taken to be equal to that at 11 μm for cloud-free regions and for overcast regions the brightness temperature at 3.7 μm is taken to be given by

$$T_{3.7} = T_{11} - 1.7K, \tag{3}$$

where T_{11} is the 11 μm brightness temperature. Brightness temperatures rather than radiances are used owing to differences in the spectral responses of the NOAA-9 and NOAA-10 AVHRRs. Relationships between brightness temperatures are likely to be similar for both instruments while relationships between the radiances are expected to differ. Unfortunately, because the NOAA-10 satellite had early morning and early evening equator crossing times, it yielded no nighttime observations like those of NOAA-9.

The empirical relationship given by (3) allows for the emissivities of clouds at 3.7 μm which are less than unity. Based on the brightness temperature at 11 μm for either overcast or cloud-free fields of view, the brightness temperature at 3.7 μm is obtained and using the spectral responses of the NOAA-9 and NOAA-10 AVHRRs the brightness temperature is converted to a radiance. The

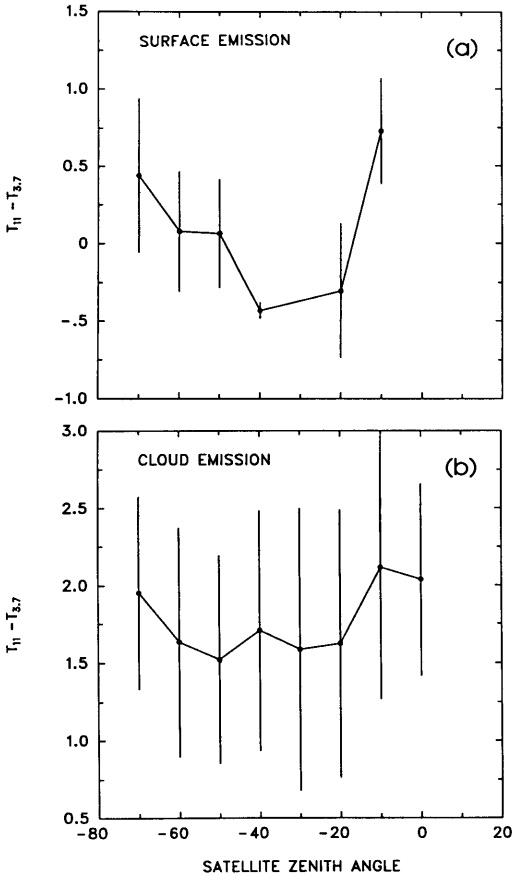

Fig. 4. Differences between 11 μm and 3.7 μm brightness temperatures for cloud-free (a) and overcast (b) regions as functions of satellite zenith angles. The observations are for the nighttime overpasses of NOAA-9 for the FIRE Marine Stratocumulus IFO.

emitted radiance is then subtracted from the observed radiance in order to obtain the reflected component. The reflectivity is taken to be given by

$$r_{3.7} = \frac{\pi I_{3.7}}{\mu_0 \pi F_{3.7}}, \tag{4}$$

where $I_{3.7}$ is the reflected component of the observed radiance; μ_0 is the cosine of the solar zenith angle associated with the observation and $\pi F_{3.7}$ is the incident solar irradiance at 3.7 μm which is taken to be 16.8 mW m^{-2} cm (Thekaekara, 1970).

Several precautions were taken to ensure the reliability of the results. First, as has already been

noted, the reflectivities of overcast clouds were compared with those of the broken clouds residing in the same $(60\ \mathrm{km})^2$ subframe. This restriction was achieved by analyzing results only for those subframes which contained a substantial number of overcast fields of view ($>10\%$) as well as a substantial number of fields of view that contained broken clouds ($>20\%$). Second, criteria were placed on the spatial coherence retrievals to ensure that the clouds in the $(60\ \mathrm{km})^2$ subframes were all from a single cloud layer. The criteria included taking only subframes from $(250\ \mathrm{km})^2$ frames which showed evidence for only one cloud layer throughout the entire frame. Furthermore, the majority of subframes which constituted the $(250\ \mathrm{km})^2$ frame satisfied the following three conditions: (1) The 10th percentile of emission for the $(4\ \mathrm{km})^2$ arrays within the subframe was consistent with the emission for overcast fields of view within the subframe. (2) The 90th percentile of the emission was consistent with the emission of either the cloud-free fields of view within the subframe or, in the event that there were no cloud-free fields of view within a particular subframe, it was consistent with the cloud-free emission that would have been obtained through interpolation from cloud-free fields of view in neighboring subframes. (3) The uncertainty in the fractional cloud cover had to be less than $0.25 \times A_c$, i.e., for $A_c = 0.4$, $\Delta A_c \leqslant 0.1$. Typically, the uncertainty in the cloud cover is ~ 0.05. The constraint therefore limits the selection of $(60\ \mathrm{km})^2$ subframes to those with $A_c > 0.2$. The uncertainty in fractional cloud cover is given by

$$\Delta A_c = \frac{\sqrt{(1-A_c)^2\,(\Delta I_s)^2 + A_c^2 (\Delta I_c)^2}}{I_s - I_c} \quad , \qquad (5)$$

where ΔI_s is the standard deviation of the emission for the cloud-free fields of view (which is either observed or interpolated from neighboring subframes) and ΔI_c is the standard deviation of the emission for overcast fields of view.

Finally, unlike the original description of the spatial coherence analysis (Coakley and Bretherton, 1982 and Coakley and Baldwin, 1984) in which the viewing angles were limited to the central portion of the scan, observations in this study were extended to the limit of the AVHRR scan angle, 55.4°, which corresponds to a satellite zenith angle of approximately 68°. No degradation in the performance of the spatial coherence method was noted for the observations at the extreme satellite zenith angles. In fact, at 11 μm the observations showed no discernible increase in fractional cloud cover with increasing satellite zenith angle. Allowing for the size of the sample and the typical variability of the fractional cloud cover, the lack of a trend in cloud cover with satellite zenith angle places an upper limit of 0.6 on the height to width ratio for the clouds observed in this study. The clouds were largely planiform.

3. Results

Figs. 5 and 6 show the solar zenith angles and azimuth angles for the reflected radiation as a function of satellite zenith angle for the collection of $(60\ \mathrm{km})^2$ subframes that survived the criteria for suitable uniform and broken layered clouds as described in the previous section. The relative azimuth angle is relative to the direction of the incident solar radiation in a plane that is parallel with the surface of the earth at the target being viewed with the indicated satellite zenith angle. The figure shows the angles collected by the NOAA-9 and NOAA-10 satellites for the FIRE Marine Stratocumulus IFO. Data analysis was restricted to ocean regions and since the California coastline was contained in each orbital pass the angles collected for the NOAA-9 satellite were primarily due to radiation reflected in the direction of forward scattering, (relative azimuth, $\phi \sim 0°$) and that for the NOAA-10 satellite were primarily due to radiation relfected in the direction of backward scattering ($\phi \sim 180°$). During the 3-week period, observations at a particular satellite zenith angle are transferable to a particular set of solar zenith and relative azimuth angles, as shown by Figs. 5 and 6. Because of the fixed relationship between satellite zenith, solar zenith and relative azimuth, results are presented as a function of satellite zenith angle only. Nevertheless, it is well to keep in mind that the results, though shown only as a function of satellite zenith angle, imply a dependence on the solar zenith and relative azimuth angles as well. Finally, because the calibrations of the NOAA-9 and NOAA-10 AVHRRs differed significantly, the results for the two satellites are presented separately.

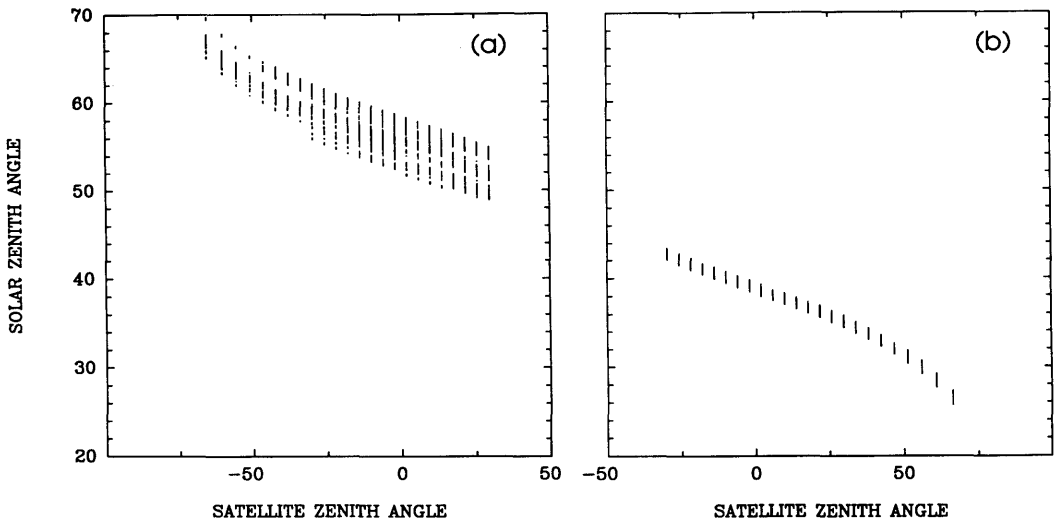

Fig. 5. Solar zenith angles as a function of satellite zenith angle for NOAA-10 (a) and NOAA-9 (b) overpasses during the FIRE Marine Stratocumulus IFO. Negative satellite zenith angles are associated with reflected radiation that is backscattered.

Fig. 7 shows the reflectivities for the cloud-free ocean background. These reflectivities are used in (1) to deduce the reflectivities of broken clouds. The values shown in the figure result from taking averages of all $(60\ \text{km})^2$ subframe values falling within the indicated satellite zenith angular bin. The average is located at the mean value for the satellite zenith angle. The error bars are the standard deviations of the subframe values falling within the indicated angular bin. The peak in the cloud-free reflectivities for NOAA-9 is due to sunglint.

Fig. 8 shows reflectivities for overcast fields of view (solid lines) and differences between the

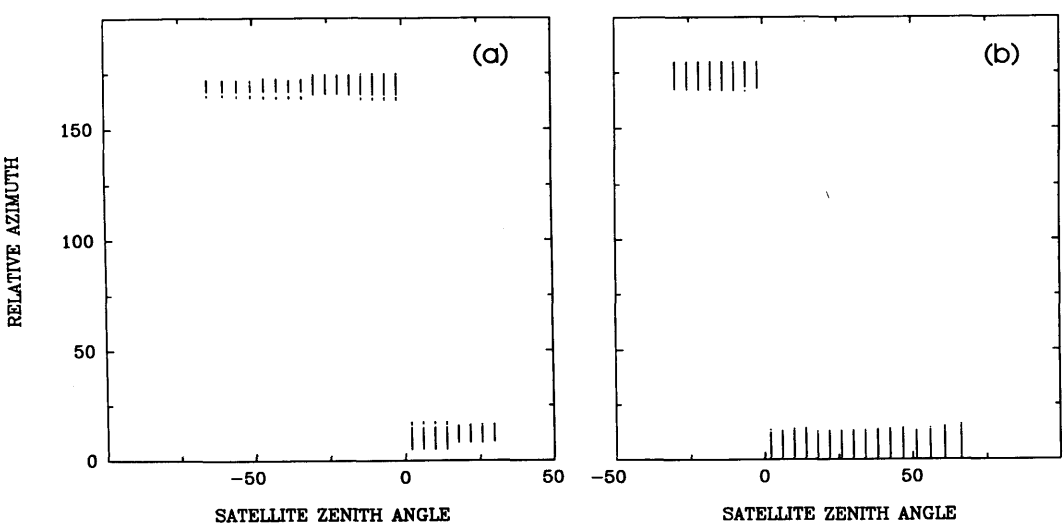

Fig. 6. Relative solar azimuths as a function of satellite zenith angle for NOAA-10 (a) and NOAA-9 (b) overpasses during the FIRE Marine Stratocumulus IFO.

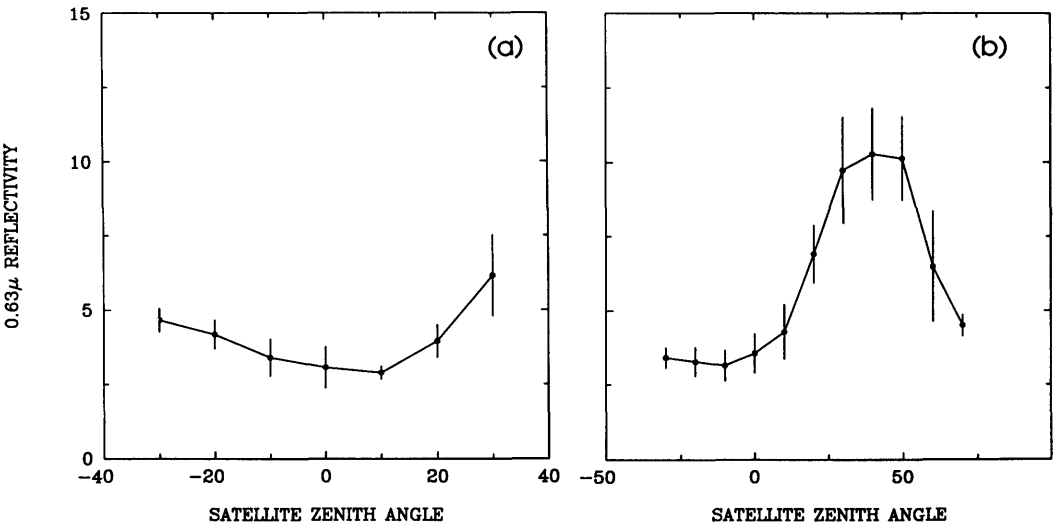

Fig. 7. 0.63 μm reflectivities of cloud-free oceans obtained for the NOAA-10 (a) and NOAA-9 (b) overpasses. The points represent means associated with the indicated satellite zenith angle; the error bars give the associated standard deviations of the observations about the means.

reflectivities of overcast and broken clouds (uniform-broken, dashed line). As with the cloud-free reflectivities the values presented are averages for all $(60\,\text{km})^2$ subframe observations falling within the indicated satellite zenith angular bin. Unlike the values for the cloud-free observations, however, the error bars in Fig. 8 represent estimates of the uncertainty in the overcast reflectivities and the differences in the reflectivities for uniform and broken clouds. These uncertainties are taken to be given by

$$\Delta r_c = \frac{2\sigma_0}{\sqrt{N}}, \tag{6}$$

where σ_0 is the standard deviation of the daily average values for the indicated satellite zenith angle and N is the number of days which contributed to the average. It is assumed that observations on a given day are highly correlated while those on different days are independent. The factor of 2 in (6) allows the error bars in Fig. 8 to indicate the range in the mean value associated with a signal-to-noise ratio of approximately 2 to 1. This ratio is approximately equivalent to the range associated with the 90% confidence limits for the value of the mean.

The ranges for the differences, as indicated by the error bars, are smaller than those for the mean reflectivities. The variability in the mean reflectivities is primarily due to variations in column liquid water amounts. Furthermore, on individual days, when the average reflectivity for overcast clouds is large, the variation in the reflectivities for overcast fields of view is also large. Likewise, when the mean reflectivity is relatively small, the variation in the reflectivities for overcast fields of view is also small. Evidently, when the amount of cloud water is large, the variation in cloud water is also large. When the amount of cloud water is small, the variation in cloud water is also small. The variability in the difference between the reflectivities for uniform and those for broken clouds, however, is limited because the difference (uniform-broken) is invariably positive, and like the case for the mean reflectivity, the variability in the difference is correlated with the magnitude of the difference. Because the differences are small compared with the mean reflectivity, the range of the difference is also small compared with the range of the mean reflectivity.

Fig. 8 indicates that at 0.63 μm the reflected radiation is nearly isotropic for the NOAA-9 satellite, for which the solar zenith angle is

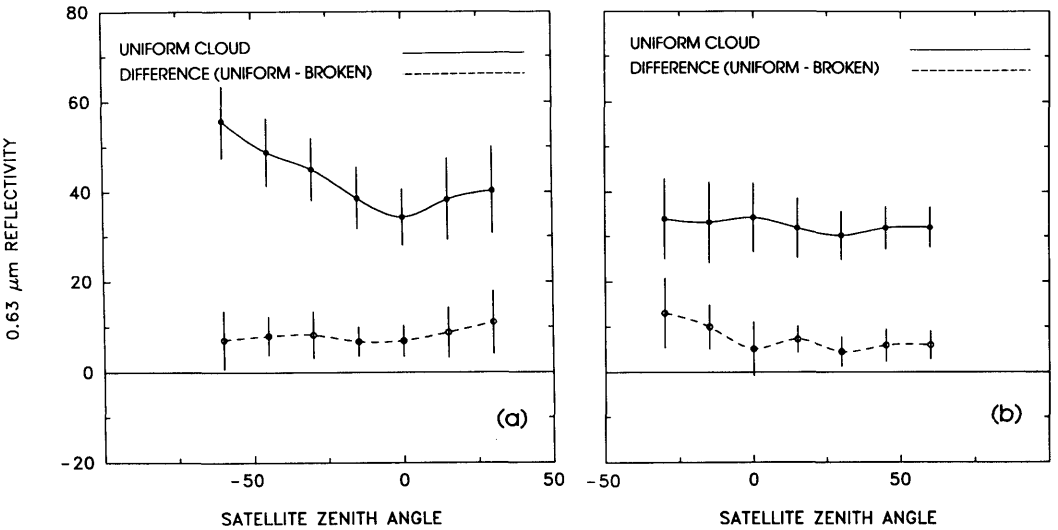

Fig. 8. 0.63 μm reflectivities of uniform clouds (solid curve, dots) and differences in reflectivities between uniform and broken clouds (uniform-broken) (dashed curve, open circles) obtained with NOAA-10 (a) and NOAA-9 (b). The points give the means; the error bars give approximate 90% confident intervals for the means.

relatively low, 25–45°, while it peaks in the backward direction for the NOAA-10 satellite, for which the solar zenith angle is relatively large, 50–65°. The peak in the backward direction is probably due to the peak in the scattering phase function for droplets with sizes typical of marine stratocumulus. The figure also shows that regardless of satellite zenith angle, reflectivities of broken clouds are significantly smaller than those of uniform clouds. With the exception of backscattered radiation for NOAA-9 observations at relatively high zenith angles, the reflectivities of broken clouds are only 80–85% of the reflectivities for uniform clouds. The lower reflectivities for broken clouds might be due to photons escaping through the sides of broken clouds and being absorbed by the surface as has been suggested by numerous simulations of radiative transfer in finite clouds (Mckee and Cox, 1974; Davies, 1978; Welch and Wielicki, 1986; Kobayashi, 1988). On the other hand, the lower reflectivities might also result from lower liquid water amounts in broken clouds as was suggested by Schmetz (1984). There is, however, no reason to rule out the possibility that both processes are occurring simultaneously.

Comparisons of the present observations with those of numerical simulations are difficult owing to the number of variables that appear to greatly influence the reflectivities of finite clouds. Optical depth, sun-target-satellite geometry, surface reflectivity, cloud shape, etc., all influence the results of numerical simulations at levels that are comparable to those calculated for the differences between uniform and broken clouds (Welch and Wielicki, 1986; Kobayashi, 1988). The differences indicated in Fig. 8 are within the range of some of the differences in albedos obtained through numerical simulation.

A striking feature of Fig. 8 is that with the possible exception of backscattered radiation observed with the NOAA-9 satellite, differences between the reflectivities of uniform and broken clouds show no differences in anisotropy. Coakley and Kobayashi (1989) point out that for a plane-parallel cloud model, differences in the anisotropies for overcast and partly cloudy scenes, if unaccounted for, will lead to 5–10% biases in the inferred radiative fluxes at the top of the atmosphere and at the surface. Such differences would amount to variations of ~0.01–0.02 for the differences between reflectivities of overcast and partly cloudy scenes as a function of satellite zenith angle. Such small differences are swamped by the sampling errors shown in Fig. 8. These sampling

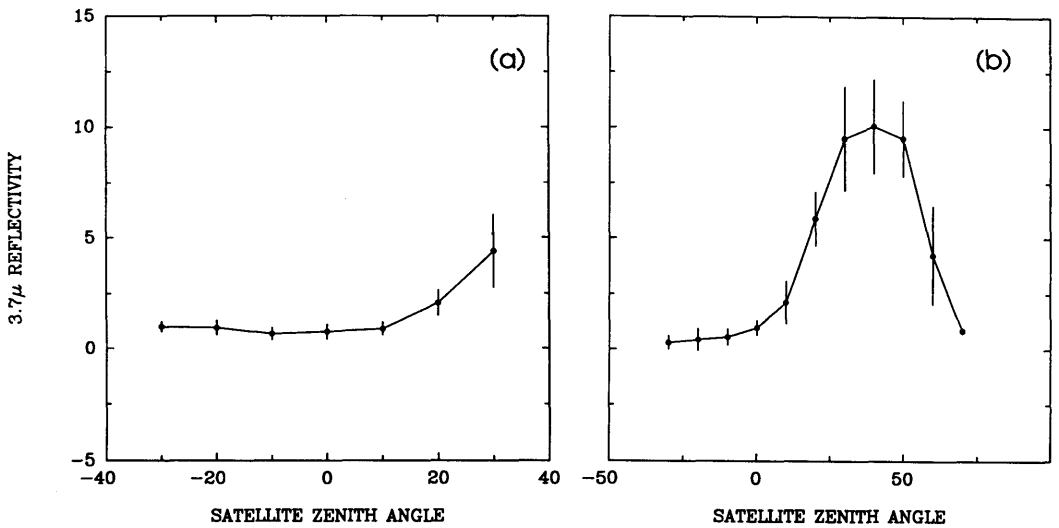

Fig. 9. Same as Fig. 7 but for 3.7 μm.

errors are inversely proportional to the square root of the number of independent samples that make up the ensemble as in (6). To reduce these errors so that they become about half the expected difference in anisotropy would require 30 to 40 times the number of cases used in the current study. That is, instead of the 10–14 days used here, observations from 300–500 days would be required to detect the anticipated differences.

Fig. 9 shows reflectivities at 3.7 μm for the cloud-free ocean background. As was mentioned in the previous section, the reflectivity at 3.7 μm is obtained by removing the contribution to the observed radiance due to thermal emission. As at 0.63 μm, sunglint is evident at 3.7 μm for radiation that is reflected in the forward direction.

Fig. 10 shows that reflectivities at 3.7 μm for uniform clouds are more anisotropic than those at

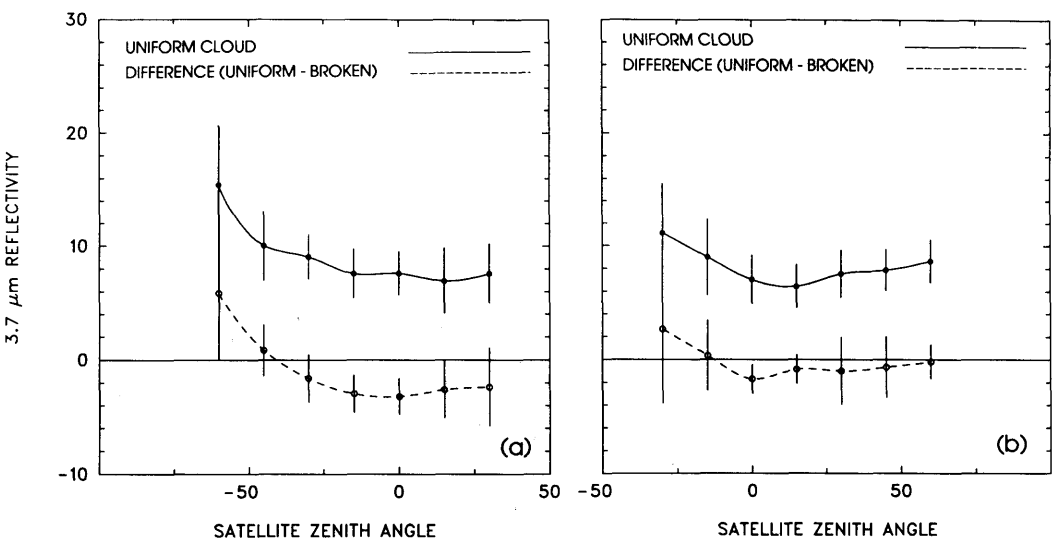

Fig. 10. Same as Fig. 8 but for 3.7 μm.

0.63 μm. The anisotropy is the result of absorption at 3.7 μm which permits only photons that have suffered low-order scattering to exit the cloud. In contrast, at 0.63 μm there is practically no absorption and the emerging photons have suffered many scatterings-thus, the term "multiple scattering."

Fig. 10 also shows differences between the reflectivities of uniform and broken clouds at 3.7 μm. As was reported by Coakley and Davies (1986), the reflectivities of broken clouds are typically higher than those of uniform clouds. With the exception of nadir satellite zenith angles, however, sampling errors all but mask the differences.

Two mechanisms may explain the enhancement of the reflectivities for broken clouds. (1) Because of low-order scattering, the reflected radiation is relatively sensitive to the orientation of the reflecting surface and the enhancements for broken clouds indicate that such clouds offer greater probabilities of surfaces that are oriented to give high reflectivities than do extensive uniform clouds. (2) Because 3.7 μm reflectivities increase with decreasing droplet size, the enhancement for broken clouds may indicate that droplet size increases systematically with distance from the edges of the clouds. As with the effects observed at 0.63 μm, there is no reason to rule out the possibility that both mechanisms may be working simultaneously.

Unlike reflectivities at 0.63 μm, those at 3.7 μm indicate that the anisotropy of reflected radiation from broken clouds is distinctly different from that for uniform clouds. While not studied, the change in the anisotropy of radiation reflected at 3.7 μm in combination with the change in the reflectivity may distinguish between the oriented-cloud-surface and shift-in-droplet-size models used here to explain the higher 3.7 μm reflectivities for broken clouds.

4. Implications

Taken together, the reflectivities at 0.63 μm and those at 3.7 μm would be consistent with plane-parallel radiative transfer calculations, if (1) clouds contained cores in which the liquid water content was high and the size of the droplets large and (2) the clouds also had edges in which the liquid water content was small and the size of the droplets was also small. An idealized model of the cloud is given in Fig. 11. The 10^2 meter scale for the cloud edge is the diffusion length of a photon at 3.7 μm for typical droplet sizes and number concentrations. It gives the depth from which a photon can emerge without being absorbed. The 1 km scale associated with the core region derives from the observation that there is considerable variability in reflectivities at 0.63 μm at 1 km, the resolution of the observations, even for uniform, overcast, layered cloud conditions. Presumably the cores are regions of updraft or buoyant plumes bringing water into the cloud from the underlying boundary layer and the surrounding edges are due to downdrafts or regions where relatively dry air above the cloud is entrained. Uniform clouds, because they exhibit large variability in reflectivities at small spatial scales, are pictured as incorporating clusters of cores which may be separated by edges in which liquid water concentrations and droplet sizes are smaller.

The systematically lower reflectivities of broken clouds at 0.63 μm could have profound implications for model estimates of the earth's albedo, such as those provided by general circulation climate models. Such model estimates fail to allow

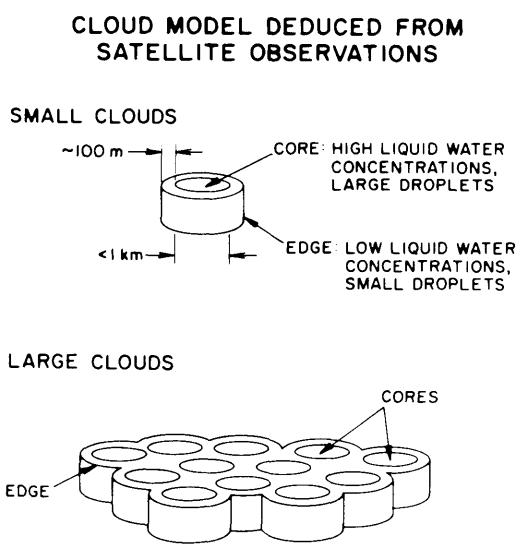

Fig. 11. Idealized model of clouds showing spatial distribution of column amounts of liquid water and droplet sizes inferred from 0.63 and 3.7 μm reflectivities for uniform and broken clouds.

for finite cloud effects, which based on the results presented here, indicate that the reflectivities of broken clouds may be only 80% of the reflectivities of their uniform counterparts. Furthermore, while large-scale observations are still being analyzed, it appears that the frequency of broken clouds at the 8 km scale, which is just resolvable by global coverage satellite imagery data, is approximately equivalent to the frequency of fractional cloud cover for 60 km regions. That is, the same fraction of 4–8 km satellite fields of view are found to be cloud-free and overcast by layered clouds as are regions that are 60 km. Global observations with the ERBE scanner for April 1985 indicate that the frequency of regions that are partly cloud covered at the resolution of the scanner ($\sim$45 km) is 60–70% (Baldwin and Coakley, 1991). So, brokenness is likely to be a dominant feature of the global cloud system.

A rough estimate of the effect of brokenness on the planetary albedo, can be obtained through the following rudimentary arithmetic. The planetary albedo is approximately given by

$$\alpha = (1 - A_c)\,\alpha_s + A_c\alpha_c, \tag{7}$$

where α_s is the mean albedo for cloud-free regions, A_c is the fractional cloud cover and α_c is the mean albedo for cloudy regions. Relationships like (7) are often used in general circulation climate models and radiative energy budget calculations. For the sake of illustration set $\alpha_s = 0.18$, $\alpha_c = 0.5$ and $A_c = 0.5$. These values give a planetary albedo of 0.34. With finite cloud effects included, the planetary albedo is given by

$$\alpha = (1 - A_c - A_c')\,\alpha_s + A_c\alpha_c + A_c'\alpha_c', \tag{8}$$

where A_c is now the fractional cloud cover associated with extensive overcast systems and A_c' is the fractional cloud cover associated with broken cloud systems. For extensive overcast systems α_c is again taken to be 0.5 but for broken cloud systems set $\alpha_c' = 0.8 \times \alpha_c = 0.4$. Based on experience with the ERBE scanner, approximately 20% of the globe is taken to be cloud-free, 20% is taken to be overcast and the remaining 60% is taken to be covered by broken clouds with $A_c' = 0.3$. The value of A_c' is set to give a total cloud cover of 0.5. With these values the planetary albedo is 0.31.

The difference in the planetary albedos given by (7) and (8) closely matches differences between pre-satellite estimates of the planetary albedo (London and Sasamori, 1971; Sasamori et al., 1971) and satellite estimates (Vonder Haar and Suomi, 1969; Raschke et al., 1973; Barkstrom et al., 1990). Of course, the estimate here is based on a limited sample of stratocumulus which hardly represents global cloud systems. Nevertheless, the results indicate that finite cloud effects are likely to prove substantial and indeed may prove sufficient to explain discrepancies between pre-satellite estimates of the planetary albedo and the value that was ultimately obtained.

Could the satellite estimates also contain significant errors because no explicit corrections are made for the effects of broken clouds? Satellite estimates of the albedo may be in error because the flux of reflected radiation, from which the albedo is derived, is itself derived from an observed radiance. The derived albedo therefore depends on estimates of the anisotropy of the reflected radiation. Since the present study was unable to detect any systematic difference in the anisotropy of the reflected radiation due to finite cloud effects, it is unlikely that substantial errors (i.e., 10%) remain in the estimate of the planetary albedo obtained from satellite observations such as those being made by ERBE, or for that matter might be inferred from the retrievals of cloud properties by the International Satellite Cloud Climatology Project. Errors due to inaccurate corrections for the anisotropy of reflected radiation will be small compared with the differences in the reflected radiation caused by differences in the reflectivities of overcast and broken cloud systems.

5. Conclusions

Satellite observations of marine stratocumulus off the coast of Southern California taken as part of the FIRE Marine Stratocumulus Intensive Field Observations, 29 June–18 July 1987 revealed that at visible wavelengths the reflectivities of broken clouds were significantly smaller than those of the same clouds where they formed regions of extensive overcast. The reflectivities of the broken clouds were only 80–85% those of the overcast clouds. As the clouds are nonabsorbing at visible wavelengths, the radiation not reflected was

transmitted to the surface. The results suggest that the pre-satellite efforts to estimate the planetary albedo may have overestimated the albedo because they failed to allow for the effects of cloud boundaries on cloud reflectivities.

At visible wavelengths no significant differences between the anisotropy of the radiation reflected by broken clouds and that reflected by the same clouds where they formed regions of extensive overcast were detected. Consequently, estimates of the planetary albedo from satellite observations are likely to be reasonably accurate. That is, errors which may arise due to errors in accounting for the effects of finite clouds on the anisotropy of the reflected radiation will be small compared with the 15–20% deficit in cloud reflectivities noted above.

As was noted earlier (Coakley and Davies, 1986), the observations made during FIRE reveal that the reflectivities of broken clouds at 3.7 μm, a wavelength at which water droplets have significant absorption, are typically larger than those of the same clouds where they form regions of extensive overcast. The reflectivities became significantly higher for near nadir viewing. Unlike the observations at visible wavelengths, the observations at 3.7 μm exhibited significant differences between the anisotropy of the radiation reflected by broken, finite clouds and that or radiation reflected by extensive overcast clouds.

These findings are consistent with the following physical processes. The deficit in reflectivity for broken clouds at visible wavelengths is consistent with the leakage of photons through the sides of clouds and their subsequent absorption by the surface. The deficit is also consistent with systematically lower amounts of liquid water for broken clouds. The higher reflectivities for broken clouds at 3.7 μm is consistent with the absorption of radiation by the cloud droplets giving rise to the reflected radiation being relatively anisotropic and consequently, rather sensitive to the orientation of the reflecting surface to the source and the observer. Broken clouds fields offer a higher probability for surfaces that exhibit high reflectivities than is offered by extensive overcast clouds. Also, there may be a systematic shift in droplet size and droplet concentration so that at the edges of clouds the sizes and numbers are small and in the interior sizes and numbers are by comparison large. Although not pursued here, it was suggested that differences in reflectivities at 3.7 μm combined with the anisotropy of radiation reflected by uniform and broken clouds may discriminate between the finite cloud effects and droplet size changes used to explain the enhanced reflectivities at 3.7 μm for broken clouds. Likewise, simultaneous observations of fractional cloud cover, cloud reflectivity and liquid water amounts could indicate whether the reduced reflectivities for broken clouds is due to their having liquid water concentrations that are smaller than those of extensive uniform clouds. Additional information on droplet size will, of course, refine such determinations. In the meantime, studies like that reported here need to be made for other regions, cloud systems and other periods to determine the extent to which the current findings are universally applicable, and to determine what effects, if any, cloud boundaries have on the anisotropy of the reflected radiation.

Acknowledgment

This work was supported in part by NASA grant NAG-1-935 for participation in FIRE.

REFERENCES

Aida, M. A. 1977. Scattering of solar radiation as a function of cloud dimension and orientation. *J. Quant. Spectrosc. Radiat. Transfer. 17*, 303–310.

Baldwin D. G. and Coakley, J. A., Jr. 1991. Consistency of ERBE bidirectional models and the observed anisotropy of reflected sunlight. *J. Geophys. Res. 96*, 5195–5207.

Barkstrom, B. R., Harrison, E. F., Lee, R. B. and the ERBE Science Team. 1990. Earth Radiation Budget Experiment preliminary seasonal results. *Eos Trans. Amer. Geophys. Union 71*, 297–312.

Coakley, J. A., Jr. and Bretherton, F. P. 1982. Cloud cover from high-resolution scanner data: Detecting and allowing for partially filled fields of view. *J. Geophys. Res. 87*, 4917–4932.

Coakley, J. A., Jr. and Baldwin, D. G. 1984. Towards the objective analysis of clouds from satellite imagery data. *J. Climate and Appl. Meteor. 23*, 1065–1099.

Coakley, J. A., Jr. and Davies, R. 1986. The effect of cloud sides on reflected solar radiation as deduced from satellite observations. *J. Atmos. Sci. 43*, 1025–1035.

Coakley, J. A., Jr. and Kobayashi, T. 1989. Broken cloud biases in albedo and surface insolation derived from satellite imagery data. *J. Climate 2*, 721–730.

Davies, R. 1978. The effect of finite geometry on the three-dimensional transfer of solar irradiance in clouds. *J. Atmos. Sci. 35*, 1712–1725.

Kobayashi, T. 1988. Parameterization of reflectivity for broken cloud fields. *J. Atmos. Sci. 45*, 3034–3045.

London, J. and Sasamori, T. 1971. Radiative energy budget of the atmosphere. *Space Research XI*, Berlin, Akad.-Verlag, 639–649.

Mckee T. B. and Cox, S. K. 1974. Scattering of visible radiation by finite clouds. *J. Atmos. Sci. 31*, 1885–1892.

Minnis, P. 1989. Viewing zenith angle dependence of cloudiness determined from coincident GOES East and GOES West data. *J. Geophys. Res. 94*, 2303–2320.

Raschke E., Vonder Haar, T. H., Bandeen, W. R. and Pasternak, M. 1973. The annual radiation balance of the earth-atmosphere system during 1969–70 from Nimbus 3 measurements. *J. Atmos. Sci. 30*, 341–364.

Reynolds, D. W., McKee, T. B. and Danielson, K. S. 1978. Effects of cloud size and cloud particles on satellite-observed reflected brightness. *J. Atmos. Sci. 35*, 160–166.

Sasamori, T., London, J. and Hoyt, D. V. 1971. Radiation budget of the Southern Hemisphere. *Meteor. Monogr. 13*, 9–22.

Schmetz, J. 1984. On the parameterization of the radiative properties of broken clouds. *Tellus 36A*, 417–432.

Thekaekara, M. P. 1970. Proposed standard values of the solar constant and the solar spectrum. *Environ. Sci. 4*, 6–9.

Vonder Haar, T. H. and Soumi, V. E. 1969. Satellite observations of the earth's radiation budget. *Science 163*, 667–669.

Welch, R. M. and Wielicki, B. A. 1986. Stratocumulus cloud field reflected fluxes: The effect of cloud shape. *J. Atmos. Sci. 41*, 3065–3103.